Applied Catalysis B: Environmental 144 (2014) 863–869

Contents lists available at ScienceDirect

Applied Catalysis B: Environmental

journal homepage: www.elsevier.com/locate/apcatb

Magnetic Fe_3O_4@C/Cu and Fe_3O_4@CuO core–shell composites constructed from MOF-based materials and their photocatalytic properties under visible light

Yong-Fei Zhang, Ling-Guang Qiu*, Yu-Peng Yuan, Yu-Jun Zhu, Xia Jiang, Juan-Ding Xiao

Laboratory of Advanced Porous Materials, School of Chemistry and Chemical Engineering, Anhui University, Hefei 230039, China

ARTICLE INFO

Article history:
Received 17 May 2013
Received in revised form 6 August 2013
Accepted 11 August 2013
Available online 28 August 2013

Keywords:
Core/shell
Magnetic
Photocatalysis
Visible light
Recyclable

ABSTRACT

Magnetic Fe_3O_4@C/Cu and Fe_3O_4@CuO nanocomposites with a core/shell structure have been successfully synthesized via direct calcinations of magnetic Fe_3O_4@HKUST-1 in different atmosphere (N_2 and air). The morphology, structure, magnetic and porous properties of the as-synthesized nanocomposites were characterized by using scanning electron microscope (SEM), transmission electron microscopy (TEM), powder X-ray diffraction (PXRD), vibration sample magnetometer (VSM), and N_2 sorption–desorption isotherms. The results show that the nanocomposite materials consist of a Fe_3O_4 core and a C/Cu (or CuO) shell. Fe_3O_4@C/Cu nanocomposites show more powerful photocatalytic activity for the degradation of methylene blue (MB) under visible light irradiation in the presence of H_2O_2 in comparison with Fe_3O_4@CuO nanocomposites and the most common photocatalyst titanium dioxide (TiO_2), as well as the recently developed organic semiconductor graphitic carbon nitride (g-C_3N_4). Meanwhile, the catalyst is stable during the reaction and the high *Ms* value (39.2 emu g^{-1}) of the as-prepared magnetic composites is favorable for the separation and recycling of the catalyst from the reaction media after the catalytic reactions.

1. Introduction

Over the past decades, size- and morphology-controlled syntheses of metal and metal oxides nanoparticles have been an extremely active area in the development of material technology not only due to their unique size- and morphology-induced physical and chemical properties that differ greatly from those of bulk materials, but also because of their various potential applications in industry and technique areas [1–3]. Among various metallic and oxide materials, copper nanoparticles (Cu NPs) and their oxides are of particular interest due to their wide applications such as magnetic storage media, solar energy transformation, electronics, sensors, batteries and catalysis [4–9]. Numerous methods such as vacuum vapor deposition (VVD), solid–vapor phase growth (SVG), microemulsion, and hydrothermal synthesis [10–15] have been developed to fabricate Cu and its oxides with various sizes and morphologies. However, to date, synthetic routes in many reports are requiring numerous and complex starting materials, reducing agents, and special additives. The intrinsic properties of Cu and its oxides, such as narrow band gap, low toxicity, good environmental acceptability, low price, and abundant resources, make it a potential candidate for photocatalytic applications. For instance Li et al. fabricated CuO nanosheets on Cu foils showing high photocatalytic efficiency on the degradation dyes [16]. Zhou et al. synthesized Cu_2O/Cu photocatalysts of heterostructure revealing excellent properties in degrading organic dyes PR, MB and MO [17]. Yu et al. reported a highly symmetric 26-facet polyhedral microcrystals of Cu_2O exhibiting good photocatalytic properties for degradation of methyl orange [18]. However, the synthesized particles are difficult to remove from solution after the photocatalytic reaction, which may increase the cost of industrial applications and repollute the treated water.

Metal-organic frameworks (MOFs) built from metal ions and polyfunctional organic ligands have attracted considerable attention due to their intriguing structures and potential application in gas storage, molecule separation, chemical sensing, catalysis, drug delivery [19–25]. MOFs with nano-sized features and supramolecular structures are ideal candidates for precursors in solid state calcination processes to fabricate nano-sized metal and metal oxides with novel structures and properties. For instance, Lin et al. used MIL-101 as a template to synthesize of octahedral Fe_2O_3/TiO_2 nanocomposite for hydrogen production from water under visible light [26]. Jung et al. obtained ZnO with ring morphology from zinc-based MOF [27]. Cho et al. synthesized Fe_3O_4 and Fe_2O_3 with rod shape from Fe-MIL-88 [28].

* Corresponding author. Tel.: +86 551 5108212; fax: +86 551 5108212.
E-mail addresses: lgqiu@ahu.edu.cn, lgahu@163.com (L.-G. Qiu).

0926-3373/$ – see front matter © 2013 Elsevier B.V. All rights reserved.
http://dx.doi.org/10.1016/j.apcatb.2013.08.019

Herein, we describe the synthesis of Fe_3O_4@C/Cu and Fe_3O_4@CuO composites via direct calcination of magnetic Fe_3O_4@HKUST-1 core–shell structures under a variety of atmospheric gaseous conditions (N_2 or air). Fe_3O_4@C/Cu possesses a relative large surface area (31.06 m^2/g). Remarkably, the Fe_3O_4@C/Cu composites show powerful photocatalytic activity in the visible band for the degradation of methylene blue (MB) in comparison with Fe_3O_4@CuO particles, and the most common photocatalyst titanium dioxide (TiO_2), as well as the more recently developed organic semiconductor graphitic carbon nitride (g-C_3N_4) [29]. Furthermore, the photocatalysts can be separated from the reaction medium under magnetic field in a few seconds and be reused for 5 cycles without obvious loss of its reactivity under visible light irradiation.

2. Experimental

2.1. Chemicals

Benzene-1,3,5-tricarboxylic acid (H_3BTC) was purchased from Aldrich. Ferric trichloride hexahydrate, cupric acetate monohydrate and mercaptoacetic acid (MAA) were purchased from Sinopharm Shanghai Chemical Reagent Co. Ltd., China. All the other chemicals used in this work were of analytical grade, obtained from commercial suppliers, and used without further purification unless otherwise noted.

2.2. Characterizations

The powder X-ray diffraction (PXRD) patterns of the prepared samples were collected using an X-ray diffractometer with Cu target (36 kV, 25 mA). Scanning electron microscope (SEM) and transmission electron microscope (TEM) analyses were conducted with a Hitachi S4800 scanning electron microscope operated at 5 kV and a JEOL JEM2100 transmission electron microscope at 200 kV, respectively. Nitrogen adsorption–desorption isotherms were obtained at 77 K on a Micromeritics ASAP 2020M+C analyzer. UV–vis diffuse reflectance data were collected with a spectrophotometer (UV-2550, Shimadzu) equipped with an integrated sphere, and $BaSO_4$ was used as a reference sample.

2.3. Synthesis of magnetic Fe_3O_4@C/Cu nanocomposites

Fe_3O_4@HKUST-1 microspheres were synthesized in accordance with the previously reported procedure [30]. Fe_3O_4@HKUST-1 (0.5 g) was placed in a ceramic boat. Then the ceramic boat was put at the middle of a horizontal quartz tube. After that the quartz tube was calcined up to 500 °C under high purity nitrogen (99.999%) atmosphere at a heating rate of 20 °C/min and then held at 500 °C for 5 h. After slow cooling to room temperature, the product was taken out and washed several times with distilled water and absolute ethanol, and finally dried in a vacuum at 60 °C for 5 h.

2.4. Synthesis of magnetic Fe_3O_4@CuO nanoparticles

All the procedures were similar to the synthesis of Fe_3O_4@C/Cu except that the sample was calcined in air atmosphere.

2.5. Photocatalytic degradation of MB

The photocatalytic activities of magnetic Fe_3O_4@C/Cu and Fe_3O_4@CuO nanocomposites were evaluated by the photodegradation of MB under a Xe lamp (XQ-500W, China) irradiation in open air and at room temperature. To measure the photocatalytic activity under UV–vis irradiation, a 420 nm cut-off filter was used to provide the visible light in this work. The distance between the light source and the beaker containing reaction mixture was fixed at 15 cm. Fe_3O_4@C/Cu or Fe_3O_4@CuO nanocomposites photocatalyst (50 mg) was put into 100 mL of MB aqueous solution (20 ppm) in a 250 mL beaker to which 3% H_2O_2 (0.5 mL) was added. The reaction suspensions were sampled at fixed time intervals and immediately magnetic separated for analysis during the reaction.

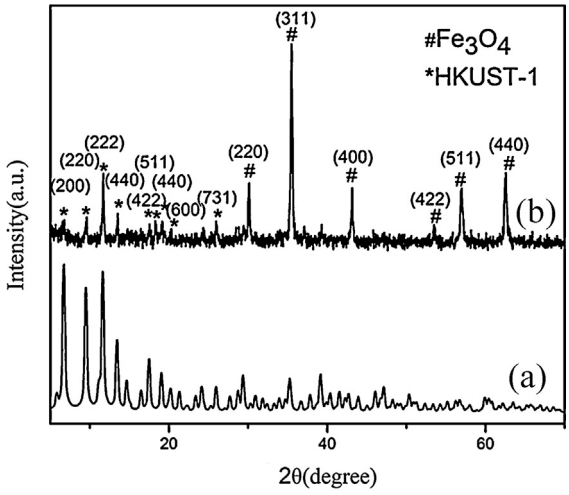

Fig. 1. PXRD patterns of (a) simulated HKUST-1 and (b) Fe_3O_4@HKUST-1 core–shell microspheres.

3. Results and discussion

3.1. Characterization of the products

The crystalline nature and composition of the as-synthesized products were first characterized by PXRD. Fig. 1 presents PXRD of the simulated HKUST-1 [31] and Fe3O4@HKUST-1. The diffraction peaks and relative intensities of Fe_3O_4@HKUST-1 core–shell microspheres in Fig. 1b can be readily indexed to crystalline Fe_3O_4 [JCPDS NO. 19-0629] and HKUST-1, respectively, indicating that the composition is composed of magnetite and HKUST-1. The weak intensity of HKUST-1 diffraction peaks can be attributed to the low thickness of the HKUST-1 shell as confirmed by TEM results shown below. All the diffraction peaks of Fe_3O_4 are well retained regardless whether the Fe_3O_4@HKUST-1 core–shell microspheres were calcined in N_2 or in air atmosphere, as shown in Fig. 2. Furthermore, the *h k l* faces including (1 1 1), (2 0 0), (2 2 0), (3 1 1), (2 2 2) of the synthesized product (Fig. S1) in the N_2 atmosphere match well with the result of the reported Cu [JCPDS NO. 04-8436], indicating that the HKUST-1 shell transformed into copper via calcination. The formation of Cu rather than CuO can be attributed to the fact that the organic ligands in the HKUST-1 shell were decomposed at high temperature into carbon and different kinds of gases including hydrogen, carbon monoxide, and benzene, together with other fragments from the incomplete decomposed ligands [32–34] which have strong reducibility. As expected, the Fe_3O_4@CuO nanoparticles were obtained by calcining Fe_3O_4@HKUST-1 in air atmosphere, which was demonstrated by the crystal faces (1 1 0) (0 0 2) (2 0 0) (0 2 0) (2 0 2) (1 1 3) of CuO [JCPDS NO. 05-0661] as shown in Fig. 2b.

The particle sizes and the morphologies of the samples were examined by using SEM and TEM. Fe_3O_4@HKUST-1 in the shape of microsphere was obtained as can be seen from the SEM images (Fig. S2), and the finally formed Fe_3O_4@HKUST-1 magnetic microspheres are composed of a Fe_3O_4 core (the black part) of about 200 nm and a HKUST-1 shell of around 80 nm, as demonstrated by TEM images (see Fig. 3a), clearly demonstrating the formation of a core–shell structure. Furthermore, the shape of the

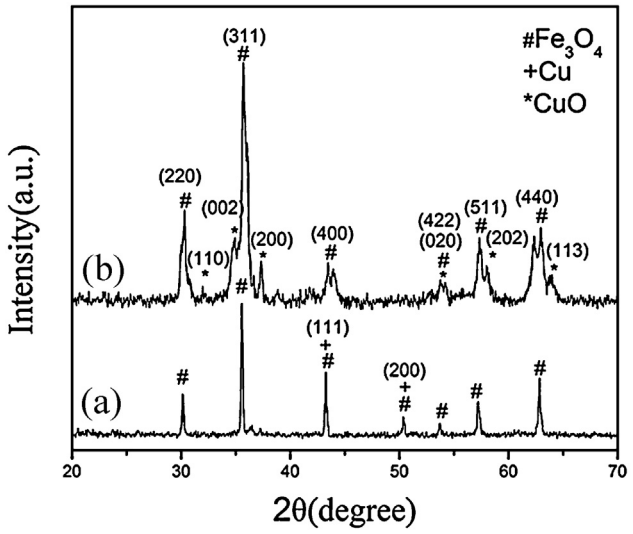

Fig. 2. PXRD patterns of nanocomposites obtained by calcination of Fe_3O_4@HKUST-1 (a) in nitrogen atmosphere and (b) in air.

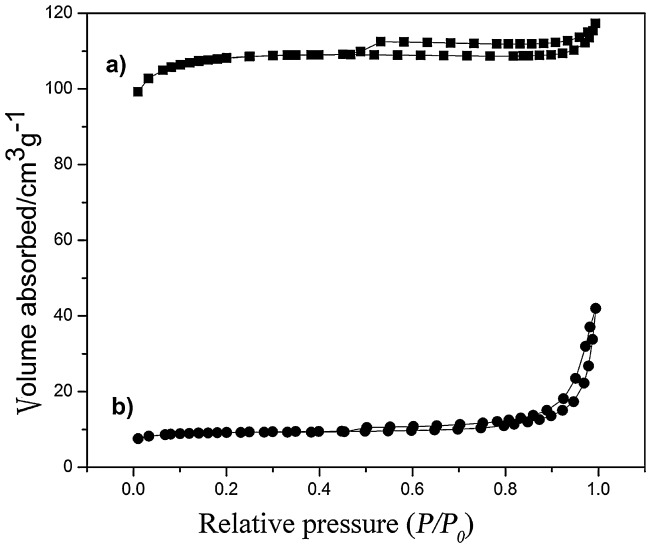

Fig. 4. N_2 sorption–desorption isotherms of (a) the as-prepared Fe_3O_4@HKUST-1 and (b) Fe_3O_4@C/Cu.

product remain unchanged and the materials still keep a core–shell structure regardless of type of the atmosphere used during the calcinations process (Fig. 3). The thickness of the C/Cu shell in Fe_3O_4@C/Cu nanospheres reduces to 50 nm in comparison with that of MOF shell in Fe_3O_4@HKUST-1 magnetic nanospheres. As can be see from Fig. 3d the Cu nanoparticles embedded in the carbon with a size ranging from 6 to 10 nm. This carbon protects the Cu nanoparticle surfaces free from the metal oxide impurity and acts as a barrier which prevents the particles from agglomerating. However, a significant decrease of shell thickness was observed after the calcinations of Fe_3O_4@HKUST-1 nanospheres in air. The thickness of CuO shell in Fe_3O_4@CuO composites is sharply decreased to 10 nm. This may be attributed to the fact that a part of carbon decomposed by organic ligands was still kept in Fe_3O_4@C/Cu, whereas shell of the Fe_3O_4@CuO nanospheres is mainly composed of CuO as confirmed by Fig. 3b.

The porous properties of magnetic samples were investigated by measuring the nitrogen adsorption isotherms, as shown in Fig. 4. The Brunauer–Emmett–Teller surface area (S_{BET}) of Fe_3O_4@HKUST-1 is determined to be 361.92 m^2/g. Compared with the other photocatalysts [35,36], the obtained Fe_3O_4@C/Cu composite possesses a relative large surface area of 31.06 m^2/g. It should be noted that S_{BET} of the products calcinated in air was as low as 0.0233 m^2/g, which imply Fe_3O_4@CuO composite is non-porous.

To evaluate the magnetic behavior of the nanocomposites, the magnetic measurements were carried out at 300 K. The magnetization saturation values (*Ms*) of the core/shell Fe_3O_4@HKUST-1, Fe_3O_4@C/Cu, Fe_3O_4@CuO were measured to be 36.5, 39.2 and

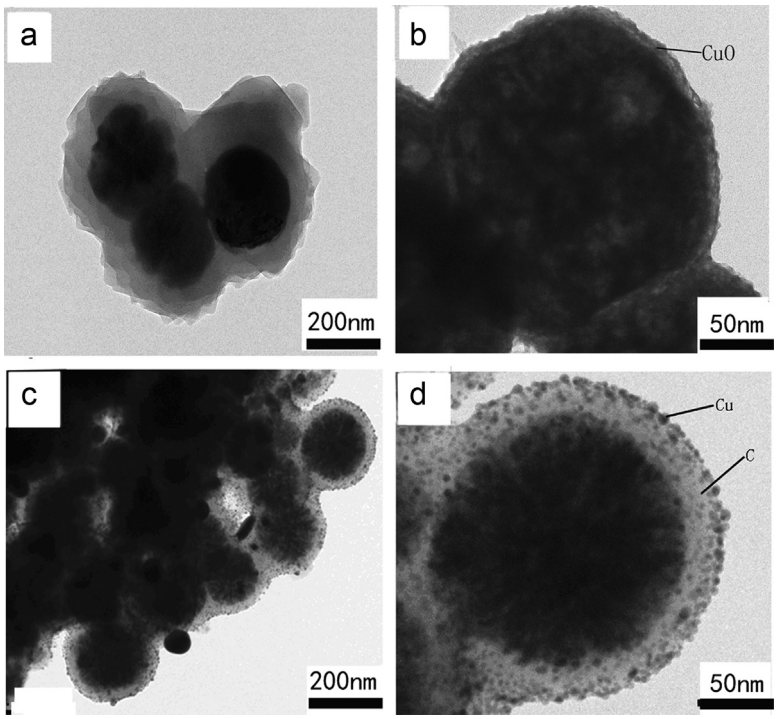

Fig. 3. TEM images of (a) Fe_3O_4@HKUST-1 core–shell microspheres, (b) Fe_3O_4@CuO, (c and d) Fe_3O_4@C/Cu.

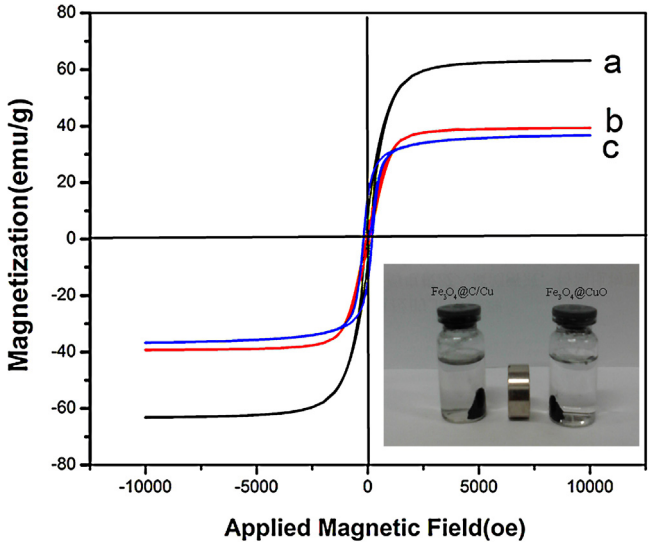

Fig. 5. Hysteresis loops recorded at 300 K of (a) Fe_3O_4@CuO, (b) Fe_3O_4@C/Cu and (c) the as-prepared Fe3O4@HKUST-1 (inset: separation of Fe_3O_4@CuO and Fe_3O_4@C/Cu from solution under an external magnetic field).

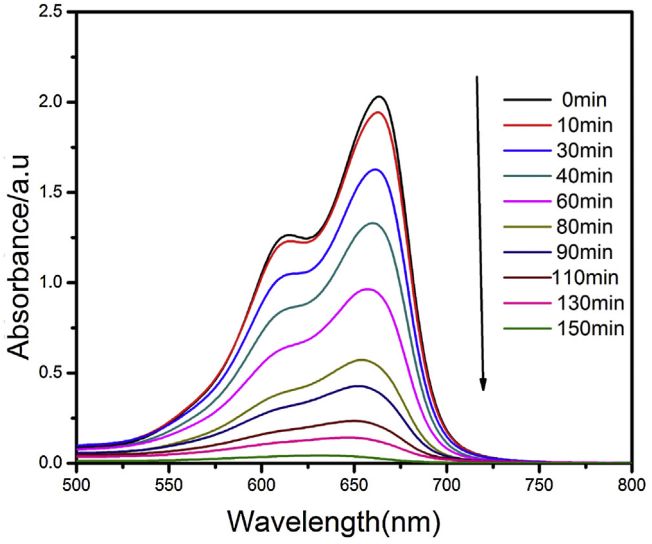

Fig. 7. UV–vis absorption spectra of MB solution with Fe_3O_4@C/Cu particles at different time intervals under visible light.

63.1 emu g^{-1}, respectively, suggesting a high magnetite content in the products (Fig. 5). The magnetic separability of Fe_3O_4@C/Cu and Fe_3O_4@CuO was tested in water by placing a magnet near the glass bottle (the inset of Fig. 5). The particles were attracted toward the magnet within few seconds, clearly demonstrating the magnetic properties of the core/shell nanocomposites.

The optical properties of the samples were investigated by UV–vis diffuse reflectances spectroscopy. Fig. 6a shows the UV–vis diffuse reflectance spectra of Fe_3O_4@C/Cu and Fe3O4@CuO. As revealed from Fig. 6a, the calcined composites showed broad absorption in the visible region. The band gap energy (E_g) was estimated from the intercept of the tangents to the plots of $(Ahv)^{1/2}$ vs photon energy [37] (Fig. 6b), and the calculated E_g value of Fe_3O_4@C/Cu is around 1.75 eV. Compared with E_g values of TiO_2 (3.2 eV) [38], g-C_3N_4 (2.7 eV) [39] and Fe_3O_4@CuO (1.82 eV) (Fig. S3), E_g value of Fe_3O_4@C/Cu is much lower, suggesting that the Fe_3O_4@C/Cu nanocomposites could sufficiently absorb visible light and may possess good photocatalytic properties when irradiated under visible light. The attribution of visible-light absorption may be due to the surface plasmon resonance (SPR) effect of Cu NPs as will be discussed below [40,41]. Metal nanocrystals can exhibit the collective oscillation of the conduction electrons upon interaction with electromagnetic radiation, which can effectively promote visible light absorption [42–44].

3.2. Photocatalytic degradation of MB

The UV–vis spectra of MB aqueous solution in the presence of Fe_3O_4@C/Cu nanocomposites under visible-light irradiation ($\lambda > 420$ nm) at room temperature for different durations to which 3% H_2O_2 (0.5 mL) was added are shown in Fig. 7. The main absorption peak at 664 nm corresponding to the MB molecule decreases rapidly with extension of the exposure time, and completely disappears after irradiation for about 150 min.

In many studies, H_2O_2 has been employed as a green additive to enhance the photocatalytic activities of photocatalysts, such as TiO_2 [45], CdS [46], and ZnO [47]. The addition of H_2O_2 was necessary for improving the photocatalytic activity of the core–shell Fe_3O_4@C/Cu nanocomposites, as shown in Fig. 8. The Fe_3O_4@C/Cu nanocomposites exhibit low photocatalytic activity in the absence of H_2O_2. However, the degradation rate increased when increasing of the amount of H_2O_2 from 0.05 mL to 1 mL. This may caused by Fe_3O_4@C/Cu nanocomposites cannot gain sufficient energy to be captured by oxygen molecules that there are little amount of O_2 was reduced by photoinduced conduction band electrons (e^-)

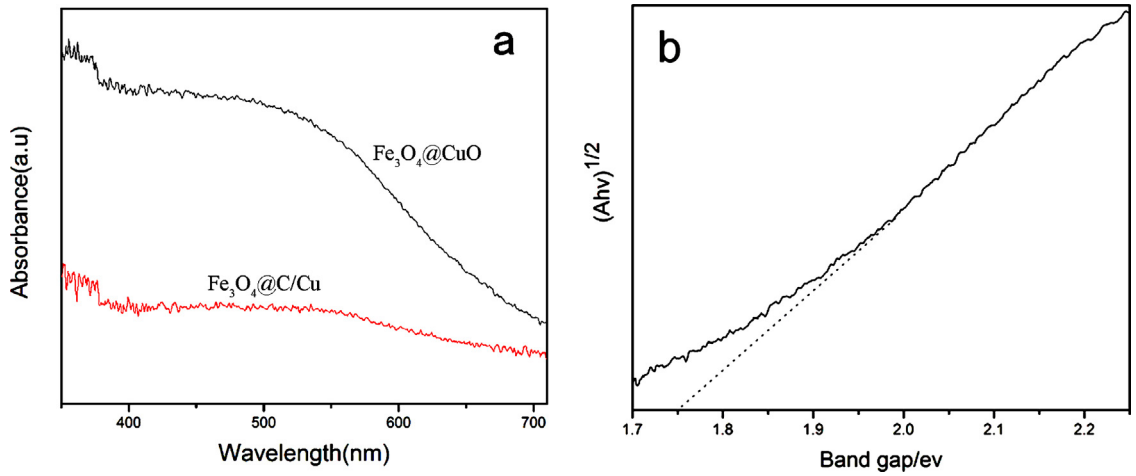

Fig. 6. (a) UV–vis diffuse reflectance spectrum of Fe_3O_4@C/Cu and Fe_3O_4@CuO. (b) Plots of $(Ahv)^{1/2}$ vs photon energy of Fe_3O_4@C/Cu.

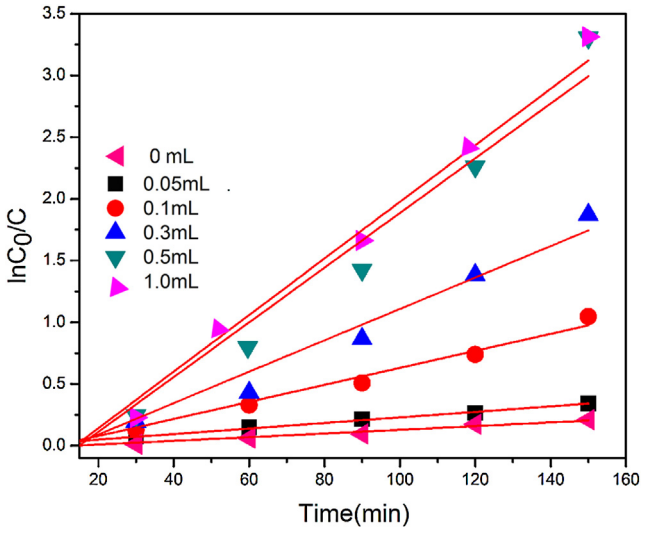

Fig. 8. Photodegradation of MB with 50 mg Fe_3O_4@C/Cu particles in the presence of various amounts of H_2O_2 under visible light.

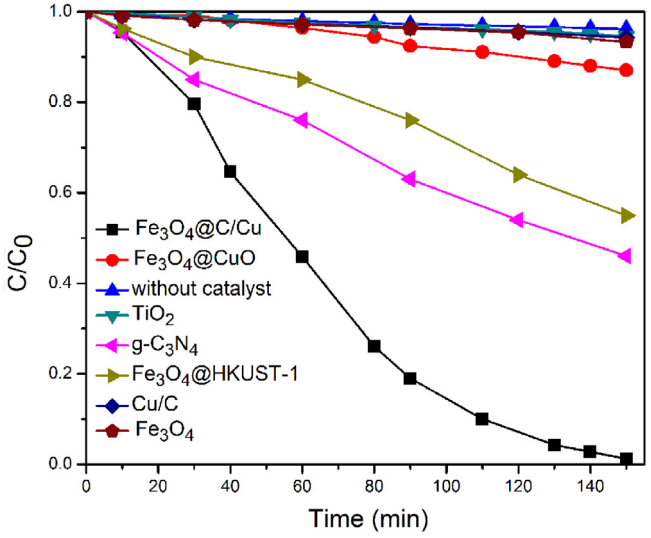

Fig. 10. Photodegradation of different catalytic conditions under visible light irradiation.

of Fe_3O_4@C/Cu to produce active oxygen species which are important for the photocatalysis. The addition of H_2O_2 can enhance the amount of the active species which mainly due to that H_2O_2 are much easier to be reduced and can be converted to •OH radicals after accepting the electrons or photolytically split directly to produce •OH which can accelerate the reaction [49,50].

The photodegradation reactions of the pollutants exhibited a modified pseudo-first-order kinetic model with respect to the irradiation time. The results were nearly consistent with the linear equation [48]:

$$\ln\left(\frac{C_0}{C}\right) = kt$$

where C_0 (mg/L) is the initial concentration of MB dye, C is the concentration of pollutant at time t, and k is the rate constant (min^{-1}).

Before photocatalysis, the porous materials were magnetically stirred under dark in the presence of H_2O_2 to ensure the adsorption/desorption equilibrium. As can be seen from Fig. 9, the Fe_3O_4@C/Cu can speedy got to a adsorption equilibrium state in 30 min, the calcination of HKUST-1 in N_2 have been reported by Bai et al. [51], and we got a product of Cu/C (see PXRD pattern in Fig. S4)

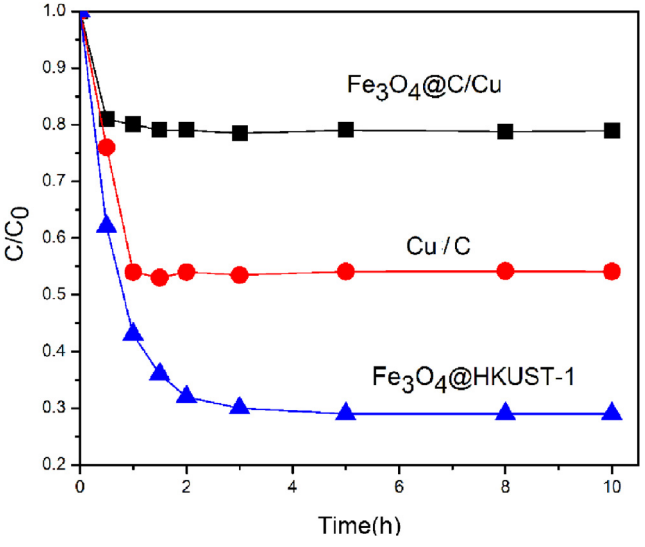

Fig. 9. The absorption of MB in the 50 mg porous materials in the presence of H_2O_2.

with a surface area of 120 m^2/g at 500 °C (Fig. S5), which can reach adsorption equilibrium in 1 h. For the Fe_3O_4@HKUST-1 composites, the adsorption capacity toward MB and the equilibrium time were both increased, which mainly due to the high surface area (361.92 m^2/g). At the same time, no photocatalysis was detected under dark for these three catalysts after reaching adsorption equilibrium.

The photocatalytic activities of all the samples obtained were studied via MB photodegradation experiments under visible light irradiation, as shown in Fig. 10. No photolysis of MB was observed after 150 min visible light irradiation in the absence of catalyst, clearly demonstrating that MB is relatively stable under visible light irradiation on the condition that there is no photocatalyst involved. The TiO_2 powder played no role in degrading MB under visible light irradiation, since TiO_2 cannot be excited by visible light irradiation. The extent of decolourization of MB was only 13% under the photocatalysis of Fe_3O_4@CuO composite, which means they possess low photocatalytic activity. Similar to previously reported results [29,52], g-C_3N_4 showed a good performance in photodegradation under visible light in the present work. However, it was obvious to find that the Fe_3O_4@C/Cu particles showed much greater degradation efficiency than g-C_3N_4 under identical conditions of exposure to visible light. For comparison, the photocatalysis of Fe_3O_4 microspheres, Fe_3O_4@HKUST-1, and the Cu/C composites were also conducted. Both Fe_3O_4 microspheres and Cu/C composites show low photocatalytic activity under the visible light even in the presence of H_2O_2. Although Fe_3O_4@HKUST-1 has a relatively good catalytic performance in the experiments, the HKUST-1 shell is not stable in water as confirmed by the PXRD (Fig.S6).

On the basis of the obtained results in the present work, a possible photocatalytic mechanism was proposed to clarify the higher photocatalytic activity of Fe_3O_4@C/Cu heterostructures than pure Fe_3O_4 microsphere and Cu/C composites in the presence of H_2O_2. The crucial obstacle limiting the efficiency of Fe_3O_4 semiconductor photocatalyst is the high rate of charge-carrier recombination which maybe due to the relatively large penetration depth of photons and the short mean free paths of charge carriers that result in a majority of the charge carriers lost to recombination before they can reach the semiconductor surface and perform photochemical reactions [53]. And it is well known that metal NPs such as gold, silver and copper NPs strongly absorb visible-light due to the so-called surface plasmon resonance (SPR) effect [54–56]. Visible light absorption heats the electrons and excites them from

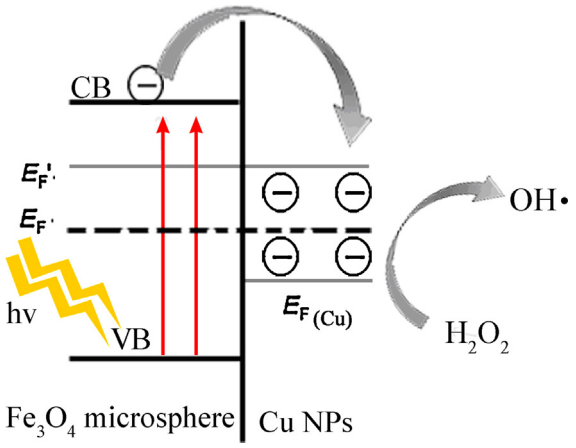

Fig. 11. Charge distribution between Fe_3O_4 microsphere and Cu NPs. EF and EF′ refer to Fermi levels of Fe_3O_4 before and after attaining equilibrium.

ground state to higher energy levels, the probability that a conduction electron participates in chemical reactions involving electron transfer is greater [57]. The existence of Cu NPs on the Fe_3O_4 microsphere core causes the Fermi level to equilibrate, which attains an energy level close to the conduction band of the Fe_3O_4 semiconductor [58]. On the other words, Cu NPs possess a low Fermi level, which can serve as a good electron acceptor for facilitating quick electron transfer from Fe_3O_4 microsphere under visible-light irradiation. Therefore, the photoexcited electrons can be rapidly transferred to Cu NPs, and the photoinduced holes still locate on Fe_3O_4 microsphere, which promote the effective separation of photoexcited electron–hole pairs and decrease the probability of electron–hole recombination. The high concentration of holes on Fe_3O_4 microsphere could significantly accelerate the photocatalytic reaction rates of organic dye degradation. On the other hand, the photocatalytic process is known to be related to the adsorption and desorption of molecules onto the surface of catalysts [59]. Carbon in the composites could adsorb the organic compounds from the aqueous solution and transfer it to the photocatalyst surface [60–62]. Additionally, carbon may carry out the role of sensitizer. The excited photosensitizer can inject an electron into the conduction band of the photocatalyst. However, under visible light irradiation, only a very small number of semiconductor@carbon/metal hetero-photocatalysts can gain sufficient energy to be captured by oxygen molecules [41], nevertheless, it can be functioned by reducing H_2O_2 into OH• (Fig. 11). As a result, the Fe_3O_4@C/Cu magnetic core/shell microspheres exhibit excellent photocatalytic activity for degradation of MB under visible-light irradiation in the presence of H_2O_2.

For the purpose of the practical applications, it is necessary to evaluate the long-term stability of photocatalyst during reaction. Stability tests were therefore performed by executing recycling reactions five times for the photodegradation of MB over Fe_3O_4@C/Cu under visible light irradiation. No obvious loss of the photocatalytic activity of Fe_3O_4@C/Cu catalyst was observed for MB decolorization (Fig. 12a), and the maximum degradation degree of MB is all close to 100% after five cycles (Fig.S7). Furthermore, PXRD patterns of Fe_3O_4@Cu before and after the reaction are shown in Fig. 12b, it can be seen that the position of the diffraction peaks remain unchanged with slightly decreasing of the peak intensities, suggesting the catalyst is relatively stable during the reaction. Meanwhile, the high *Ms* values of the as-prepared magnetic composites were favorable for the separation and recycling of the catalyst from the reaction media after the catalytic reactions.

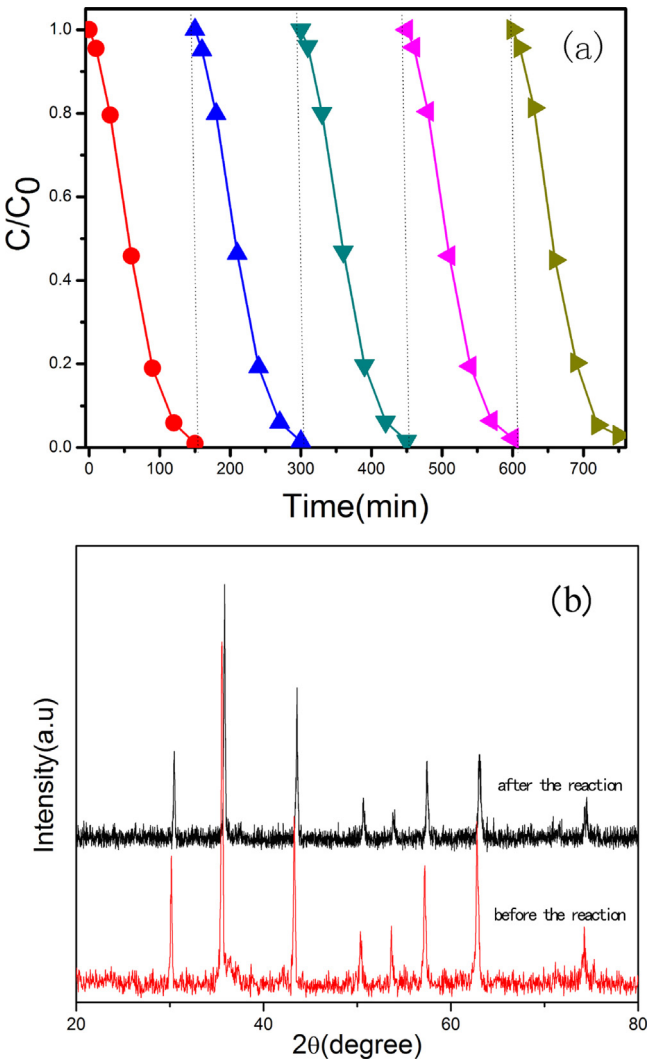

Fig. 12. (a) Catalyst recycling in the degradation of MB of Fe_3O_4@C/Cu. (b) PXRD patterns for Fe_3O_4@C/Cu before and after the reaction.

4. Conclusions

In summary, we demonstrate a simple synthetic route for the synthesis of core–shell-structured magnetic Fe_3O_4@C/Cu and Fe_3O_4@CuO nanocomposites via direct calcination of magnetic Fe_3O_4@HKUST-1 in different atmosphere (N_2 and air). Compared with other reported methods, the advantage of this synthetic route lies in its simplicity including easy synthesis, environmental friendliness with use of a benign magnetic MOF precursor, as well as without using any reductives. Meanwhile, Fe_3O_4@C/Cu possesses a relative large surface area. This synthetic method presented here can be extended to the synthesis of other porous magnetic metal or metallic oxide from MOF based materials. Remarkably, the Fe_3O_4@C/Cu magnetic core/shell microspheres exhibit excellent photocatalytic activity for degradation of MB in comparison with Fe_3O_4@CuO, g-C_3N_4, and TiO_2 powders under visible-light irradiation in the presence of H_2O_2. Furthermore, the magnetic nature of the Fe_3O_4@C/Cu magnetic core/shell structured photocatalyst promotes its easy separation from the reaction media by simple application of an external magnetic field, and the photocatalyst could be reused for 5 cycles without obvious loss of its reactivity under visible light irradiation. The simple procedures for both preparation and the recovery of the photocatalyst and excellent recycling efficiency of the catalyst make it an ideal photocatalytic

system for the photodegradation of organic pollutants under visible light from waste water in industry.

Acknowledgments

This work was supported by the National Natural Science Foundation of China (20971001, 51002001 and 20371002), the NSFC-CAS Joint Fund for Research Based on Large-Scale Scientific Facilities (10979014), the Program for New Century Excellent Talent in University, Ministry of Education, China (NCET-08-0617), and the"211 Project" of Anhui University.

Appendix A. Supplementary data

Supplementary data associated with this article can be found, in the online version, at http://dx.doi.org/10.1016/j.apcatb.2013.08.019.

References

[1] B. Bhushan, Springer Handbook of Nanotechnology, Springer, Berlin, Heidelberg, New York, 2007.
[2] Q. Zhang, S.J. Liu, S.H. Yu, J. Mater. Chem. 19 (2009) 191–207.
[3] C.N.R. Rao, A. Müller, A.K. Cheetham, Nanomaterials Chemistry: Recent Developments and New Directions, Wiley-VCH, 2007.
[4] P.C. Dai, H.A. Mook, G. Aeppli, et al., Nature 406 (2000) 965–968.
[5] S. Harikrishnan, S. Kalaiselvam, Thermochim. Acta 533 (2012) 46–55.
[6] A.A. Ali, A.K. Al-Asmari, Appl. Nanosci. 2 (2012) 55–61.
[7] L.Q. Mao, K. Yamamoto, W.L. Zhou, L.T. Jin, Electroanalysis 12 (2000) 72–77.
[8] P. Poizot, S. Laruelle, S. Grugeon, L. Dupont, J.-M. Tarascon, Nature 407 (2000) 496–499.
[9] Z.F. Chen, T.J. Meyer, Angew. Chem. 125 (2013) 728–731.
[10] Z.W. Liu, Y. Bando, Adv. Mater. 15 (2003) 303–305.
[11] B. Liu, H.C. Zeng, J. Am. Chem. Soc. 126 (2004) 8124–8125.
[12] Y. Liu, Y. Chu, Y. Zhuo, L. Dong, L. Li, M. Li, Adv. Funct. Mater. 17 (2007) 933–938.
[13] C. Salzemann, A. Brioude, M. Pileni, J. Phys. Chem. B 110 (2006) 7208–7212.
[14] M. Cao, C. Hu, Y. Wang, Y. Wang, Y. Guo, C. Guo, E. Wang, Chem. Commun. 6 (2003) 1884–1885.
[15] Y. Xu, D. Chen, X. Jiao, J. Phys. Chem. B 109 (2005) 13561–13566.
[16] F. Li, X.Q. Liu, Q. Zhang, T. Kong, H.J. Jin, Cryst. Res. Technol. 47 (2012) 1140–1147.
[17] B. Zhou, Z.G. Liu, H.X. Wang, Y.Q. Yang, W.H. Su, Catal. Lett. 13 (2009) 75–80.
[18] W. Zhou, B. Yan, C. Cheng, C. Cong, H. Hu, H. Fan, T. Yu, CrystEngComm 11 (2009) 2291–2296.
[19] Y.H. Hu, L. Zhang, Adv. Mater. 22 (2010) E117–E130.
[20] J.W. Yoon, S.H. Jhung, Y.K. Hwang, S.M. Humphrey, P.T. Wood, J.S. Chang, Adv. Mater. 19 (2007) 1830–1834.
[21] L.G. Qiu, Z.Q. Li, Y. Wu, W. Wang, T. Xu, X. Jiang, Chem. Commun. (2008) 3642–3644.
[22] J.Y. Lee, O.K. Farha, J. Roberts, K.A. Scheidt, S.T. Nguyen, J.T. Hupp, Chem. Soc. Rev. 38 (2009) 1450–1459.
[23] A. Corma, H. García, F.X. Llabrés, I. Xamena, Chem. Rev. 110 (2010) 4606–4655.
[24] P. Horcajada, C. Serre, M. Vallet-Regí, M. Sebban, F. Taulelle, G. Férey, Angew. Chem. Int. Ed. 45 (2006) 5974–5978.
[25] K.M.L. Taylor-Pashow, J.D. Rocca, Z.G. Xie, S. Tran, W.B. Lin, J. Am. Chem. Soc. 131 (2009) 14261–14263.
[26] K.E. Krafft, C. Wang, W.B. Lin, Adv. Mater. 24 (2012) 2014–2018.
[27] S. Jung, W. Cho, H.J. Lee, M. Oh, Angew. Chem. Int. Ed. 48 (2009) 1459–1462.
[28] W. Cho, S. Park, M. Oh, Chem. Commun. 47 (2011) 4138–4140.
[29] X.C. Wang, K. Maeda, A. Thomas, K. Takanabe, G. Xin, J.M. Carlsson, K. Domen, M. Antonietti, Nat. Mater. 8 (2009) 76–80.
[30] F. Ke, L.G. Qiu, Y.P. Yuan, X. Jiang, J.F. Zhu, J. Mater. Chem. 22 (2012) 9497–9500.
[31] M. Maes, L. Alaerts, F. Vermoortele, R. Ameloot, S. Couck, V. Finsy, J.F.M. Denayer, D.E. Devos, J. Am. Chem. Soc. 132 (2010) 2284–2292.
[32] W. Schmitt, J.P. Hill, S. Malik, C.A. Volkert, I. Ichinose, C.E. Anson, Angew. Chem. Int. Ed. 44 (2005) 7048–7053.
[33] L.Y. Chen, J.F. Bai, C.Z. Wang, Y. Pan, M. Scheer, X.Z. You, Chem. Commun. 11 (2008) 1581–1583.
[34] R. Das, P. Pachfule, R. Banerjee, P. Poddar, Nanoscale 4 (2012) 591–599.
[35] Z.Y. Xiong, L.L. Zhang, X.S. Zhao, Chem. Eur. J. 17 (2011) 2428–2434.
[36] S. Ye, L.G. Qiu, Y.P. Yuan, Y.J. Zhu, J. Xia, J. Mater. Chem. A 1 (2013) 3008–3015.
[37] F. Dong, L.W. Wu, Y.J. Sun, M. Fu, Z.B. Wu, S.C. Lee, J. Mater. Chem. 21 (2011) 15171–15174.
[38] H. Zcaron, V. Církva, O. Solcova, M. Hajek, J. Chem. Technol. Biotechnol. 84 (2009) 1624–1630.
[39] G.Z. Liao, S. Chen, X. Quan, H.T. Yu, H.M. Zhao, J. Mater. Chem. 22 (2012) 2721–2726.
[40] L.M. Liz-Marzan, Langmuir 22 (2006) 32–41.
[41] X. Chen, Z.F. Zheng, X.B. Ke, E. Jaatinen, T.F. Xie, D.J. Wang, C. Guo, J.C. Zhao, H.Y. Zhu, Green Chem. 12 (2010) 414–419.
[42] C. Hu, T. Peng, X. Hu, Y. Nie, X. Zhou, J. Qu, H. He, J. Am. Chem. Soc. 132 (2010) 857–862.
[43] X. Fang, Y. Bando, U. Gautam, C. Ye, D. Golberg, J. Mater. Chem. 18 (2008) 509–522.
[44] Z. Zheng, B. Huang, X. Qin, X. Zhang, Y. Dai, M. Whangbo, J. Mater. Chem. 21 (2011) 9079–9087.
[45] N.M. Mahmoodi, M. Arami, N.Y. Limaee, N.S. Tabrizi, J. Colloid Interface Sci. 295 (2006) 159–164.
[46] Y.Y. Huang, F.Q. Sun, T.X. Wu, Q.S. Wu, Z. Huang, H. Su, Z.H. Zhang, J. Solid State Chem. 184 (2011) 644–648.
[47] N. Daneshvar, D. Salari, A.R. Khataee, J. Photochem. Photobiol. A 162 (2004) 317–322.
[48] Y.L. Zheng, D.L. Liu, S.W. Liu, S.Y. Xu, Y.Z. Yuan, L. Xiong, J. Environ. Sci. 21 (2009) 1194–1199.
[49] G.D. Lee, S.K. Jung, Y.J. Jeong, J.H. Park, C.S. Suh, B.H. Ahn, S.S. Hong, J. Ind. Eng. Chem. 8 (2002) 22–27.
[50] Y.K. Takahara, Y. Hanada, T. Ohno, S. Ushiroda, S. Ikeda, M. Matsumura, J. Appl. Electrochem. 35 (2005) 793–797.
[51] L.Y. Chen, Y.M. Shen, J.F. Bai, C.Z. Wang, J. Solid State Chem. 182 (2009) 2298–2306.
[52] S.C. Yan, Z.S. Li, Z.G. Zou, Langmuir 25 (2009) 10397–10401.
[53] K. Zhu, N.R. Neale, A. Miedaner, A.J. Frank, Nano Lett. 7 (2007) 69–74.
[54] H. Yuan, Chem. Mater. 19 (2007) 1592–1600.
[55] X.H. Huang, I.H. El-Sayed, W. Qian, M.A. El-Sayed, J. Am. Chem. Soc. 128 (2006) 2115–2120.
[56] L. Kelly, E. Coronado, L.L. Zhao, G.C. Schatz, J. Phys. Chem. B 107 (2003) 668–677.
[57] X. Chen, Z.F. Zheng, X.B. Ke, E. Jaatinen, T.F. Xie, D.J. Wang, C. Guo, J.C. Zhao, H.Y. Zhu, Green Chem. 12 (2010) 414–419.
[58] T. Hirakawa, P.V. Kamat, J. Am. Chem. Soc. 127 (2005) 3928–3934.
[59] Y.W. Wang, L.Z. Zhang, S. Li, P. Jena, J. Phys. Chem. C 113 (2009) 9210–9217.
[60] B. Tryba, A.W. Morawski, M. Inagaki, Appl. Catal. B 41 (2003) 427–433.
[61] T. Tsumura, N. Kojitani, M. Toyoda, M. Inagaki, J. Mater. Chem. 12 (2002) 1391–1396.
[62] M. Janus, B. Tryba, M. Inagaki, A.W. Morawski, Appl. Catal. B 52 (2004) 61–67.